Hydrothermal synthesis of nanosized $BaTiO_3$ powders and dielectric properties of corresponding ceramics

Madona Boulos, Sophie Guillemet-Fritsch, François Mathieu, Bernard Durand, Thierry Lebey and Vincent Bley

Centre Inter-Universitaire de Recherche et d'Ingénierie des Matériaux (CIRIMAT) Bât. 2R1. Université Paul Sabatier, 118, route de Narbonne, 31062 Toulouse Cedex 04, France
Laboratoire de Génie Electrique de Toulouse (LGET) Bât. 3R3, Université Paul Sabatier, 118, route de Narbonne, 31062 Toulouse Cedex 04, France

Abstract

$BaTiO_3$ fine powders were synthesized by hydrothermal method at 150 °C or 250 °C for 7 h, starting from a mixture of $TiCl_3$ + $BaCl_2$ or TiO_2 + $BaCl_2$. The size of the crystallites is close to 20 nm whatever the starting mixture and the reaction temperature. These powders are well crystallized and constituted of a mixture of the metastable cubic and stable tetragonal phases. The ceramics obtained after uniaxial pressing and sintering at 1250 °C for 10 h or 20 h present high densification (up to 99.8%). The Curie temperature (T_c) and the electrical permittivity (ε_r) of the ceramics strongly depend on the type of titanium source that has been used for preparing the powder and on the sintering dwell time. Particularly, T_c is shifted towards lower temperature when $TiCl_3$ is used. The permittivity value at T_c of $BaTiO_3$ sintered at 1250 °C for 10 h reaches 7000 and 11,000 with respectively $TiCl_3$ and TiO_2 used as titanium source.

Keywords: Barium titanate; Hydrothermal synthesis; Electrical properties

1. Introduction

$BaTiO_3$ is an ubiquitous electronic ceramic, widely utilized in the manufacture of thermistors, multilayer ceramic capacitors (MLCCs) and electro-optic devices [1]. Recently, with

the miniaturization of electronic devices, the down sizing of MLCCs has been developed and accelerated. For this purpose, it is expected to decrease the thickness of the dielectric layers to values less than 1 μm. Consequently, $BaTiO_3$ raw materials with elementary particle size from a few hundred nm to a few ten nm are needed so as a significant number of particles constitute the layer [2], [3] and [4]. The decrease of ferroelectric properties with decreasing particle size, evidencing a critical size below which the ferroelectric state no more exists whatever the temperature, has been widely studied [5], [6], [7], [8], [9] and [10], as well as the influence of the particle size on the relative permittivity ε_r [2] and [11].

Traditionally, $BaTiO_3$ is prepared by solid state reaction via the calcination of $BaCO_3$ and TiO_2. The temperature needed is as high as 800 to 1200 °C. The powders are highly agglomerated and they require extensive milling before they can be used in the various forming processes [12]. However, chemically homogeneous BT powders can be prepared by calcination of equimolar mixtures of submicronic $BaCO_3$ (d_{50} = 0.17 μm) and TiO_2 (d_{50} = 0.20 μm) at 900 °C for a few hours [13]. The powders obtained are in the form of micronic aggregates of submicrometer crystallites, which according to the authors can be easily desintegrated to particle sizes $d_{50} < 0.4$ μm in a ball-mill. So, the solid-state preparation of dielectric powders with crystallite sizes close to 0.2 μm, using submicrometer raw materials, can be a promising alternative to more expensive wet chemical preparation routes. Nevertheless, the wet chemical preparation routes have been intensively investigated because they allow a better control of the granulometric distribution and offer the possibility for the synthesis of highly pure, homogeneous, ultrafine and multicomponent powders: sol–gel process [14], [15], [16], [17], [18] and [19], oxalate route giving particle size close to 25 nm when calcination is performed in air at 700 °C [10] and particle size in the range 15–20 nm when thermal treatment is carried out first at 400 °C for 1 h under O_2 flow and then at temperature from 550 to 750 °C for 0.5 h under vacuum [20], micro-emulsion process [21] and [22], polymeric precursor method [23] and hydrothermal method [24], [25], [26], [27], [28], [29], [30], [31], [32], [33], [34], [35], [36], [37], [38], [39], [40], [41], [42] and [43]. The hydrothermal synthesis of ceramic powders is of great interest because of the possibility of producing highly crystallized, well dispersed and sintering-active powders. One of its advantages is that conventional teflon-lined stainless steel bombs can be used. Hence, it can be called upon to highly caustic solutions for the synthesis of $BaTiO_3$.

The polymorphic variety obtained (metastable cubic or tetragonal) depends upon the synthesis parameters (temperature, presence of counter anions) and the characteristics of the powders (size of crystallites, presence of defects). Hennings [24] reported the hydrothermal preparation, from barium–titanium–acetate precursors, of highly crystallized cubic BT powders having a size 0.2 to 0.3 μm. However, the hydrothermal synthesis involves typically the reaction of $Ba(OH)_2$ or $BaCl_2.2H_2O$ as barium source and titanium alcoxide or TiO_2 as titanium source.

The reaction has to be carried out in a strongly alkaline solution (0.1 M OH^- or above) and crystalline powder is reported to form in the temperature range 85–250°C within a couple of hours. Below 250 °C and in absence of halide ions, especially chloride, a metastable cubic polymorph is obtained and has to be annealed at temperatures exceeding 1000 °C in order to stabilize the tetragonal form upon cooling [40], [41] and [42]. The crystallite size is close to 0.2 μm [40]. According to Christensen [29], the tetragonal form, thermodynamically stable at room temperature, can be directly synthesized by the hydrothermal method, using $Ba(OH)_2$ and oxides, esters or oxide gels of titanium as precursors, on the condition to carry out the reaction at a temperature in the range 450–600 °C, significantly higher than 250 °C; the process was favoured at the highest temperature. Dutta [40] synthesized the tetragonal polymorph at only 240 °C, but introducing Cl^- ions in the hydrothermal medium, using either $BaCl_2$ and TiO_2 as metal sources or using $Ba(OH)_2$ and TiO_2 as metal sources and adding NaCl to the medium. The formation of

the tetragonal variety is partly explained by the increase of the size of crystallites from 0.2 to 1.0 μm. This observation is corroborated by Wei-Lu [43] who tailored cubic BT crystals, with sizes close to 0.08 μm, by hydrothermal method starting from aqueous solutions of $BaCl_2$ and $TiCl_4$ at 250 °C for 0.5–2.0 h, but adding polyoxyethylen sorbitan monoleate as a polymeric surface modifier.

In the tetragonal BT, the TiO_6 octahedra have to be completely distorted with a displacement of the Ti^{4+} ions of about 0.12 Å and a displacement of oxygen of approximately 0.03 Å [45]. The strains linked to the distortion need large crystallites to be accommodated. Consequently, in nanosized BT crystallites, the distortion leading to the cubic-to-tetragonal phase transition, by cooling the sample through the Curie temperature, is not possible and the metastable cubic polymorph is obtained. In fact, the nanocrystallites are so small that the surface defects become predominant compared to the bulk ones and prevent the completion of the structural transition leading to high strains within the crystal [32]. Viekanandan [31] suggested that the strains in the crystallites are related to point defects in the lattice. Xia [42] assumed that the abnormal crystallographic features result from defects caused by OH^- incorporated in the perovskite lattice. Wada [20] evidenced OH^- and CO_3^{2-} groups adsorbed on the surface of crystallites but no lattice OH^- in 17 nm sized cubic BT. Shi [38] also reported that the stabilization of cubic BT is caused by defects including OH^- defects and barium vacancies and indicated that the formation of tetragonal BT is promoted by the use of a molar ratio Ba/Ti = 3 in the hydrothermal medium which reduces the probability of forming barium vacancies.

In this paper, we report various physical and chemical characteristics of $BaTiO_3$ powders synthesized by the hydrothermal method using two different titanium sources, $TiCl_3$ and TiO_2. They are discussed from the nature of titanium salt. The barium source was $BaCl_2{\cdot}2H_2O$. The synthesis was performed at two temperatures, namely 150 °C and 250 °C. Finally, the electrical properties of the corresponding ceramics are presented and correlated to the powders and ceramics characteristics.

2. Experimental procedure and characterization

The starting materials were barium chloride ($BaCl_2{\cdot}2H_2O$, Prolabo 99%), titanium trichloride ($TiCl_3$, Prolabo, d = 1.20, % min = 15%) and titanium dioxide (TiO_2 anatase, Rhodia). $TiCl_3$ was preferred to $TiCl_4$ because it is less sensitive to moisture. Indeed in presence of moist air, liquid $TiCl_4$ (m.p. = −25 °C) releases thick white smokes due to the formation of finely divided titanium oxichloride; it is a well-known smoke material. On the opposite, solid $TiCl_3$ can be easily dissolved in water and the hydrolysis prevented by acidification. So an acid solution of $TiCl_3$ is more easy to handle than liquid $TiCl_4$. An aqueous solution of barium and titanium chlorides was obtained by mixing 0.015 mol $TiCl_3$ or TiO_2 and 0.024 mol $BaCl_2{\cdot}2H_2O$ in deionised water. Our experiments proved that the formation of $BaTiO_3$ was promoted by an initial precursor molar ratio Ba/Ti = 1.6. The solution pH was raised up to 13.5 by adding a solution of KOH under stirring. Potassium hydroxide was used rather than sodium hydroxide because the size of K^+ ions (d = 0.266 nm), strongly larger than that of Na^+ ions (d = 0.190 nm), makes its fixation in the $BaTiO_3$ lattice more difficult. The suspension obtained was transferred into a cylindrical autoclave (Paar, teflon lined stainless steel) filled at 2/3 of its volume. The autoclave was put inside a preheated regulated oven and the reaction was performed for 7 h at 150 or 250 °C under autogeneous pressure (5 to 39 bars). After cooling at room temperature, the water

insoluble reaction product was washed with a solution 0.1 M HCl to remove the $BaCO_3$ that is present beside $BaTiO_3$ at the end of the hydrothermal treatment, then filtered, washed several times with distilled water and oven dried at 110 °C for 24 h.

ICP (Inducted Coupled Plasma) measurements were used to determine the barium, titanium and potassium contents in the powder. The amount of chloride ions was estimated by HPLC (High performance liquid chromatography). The structure was identified using X-ray diffractometry at room temperature (Siemens D 501 diffractometer equipped with a SiLi detector, $\lambda_{CuK\alpha}$ = 1.5418 Å) in the 2θ range 20°–80° at a scan rate of 0.03°/min. Microstructural studies of powders were performed using electron microscopy (Jeol JSM 6700F SEM-FEG). The mean size of crystallites, d_x, was calculated from the broadening of the XRD peaks using the Scherrer formula [44]:

$$d_x = 0.94\lambda/\beta\cos\theta \quad (1)$$

where d_x is the crystallite mean size, λ the wavelength, β the true full width at half maximum and θ the diffraction angle of the center of the peak (in degrees).

The powder specific surface area was measured by nitrogen desorption according to the BET method (Micromeritics Desorb 2300 A/Flow sorb II 2300). Assuming that the powders are constituted of monosized and non-porous spherical particles, their geometrical surface is related to the diameter by relation (2):

$$S = 6/\rho d \quad (2)$$

S is the geometric surface ($cm^2 \cdot g^{-1}$); d is the particle diameter (cm) and ρ the theoretical specific mass (6.02 $g.cm^{-3}$). The comparison of the geometric surface, calculated either from the mean diameter of crystallites obtained by XRD peaks broadening or from the particle diameter determined by electron microscopy, with the specific surface area measured by BET gives indications on the porosity or the nature of elementary grains (mono or poly-crystalline).

Raman investigations were carried out by means of a DiLor XY Micro Raman Spectrometer equipped with a Princeton Instruments LN/CCD detector. Thermogravimetric analyses were performed using a Setaram 92 thermobalance (heating rate 5 $°C \cdot h^{-1}$, air flowing 0.8 $L \cdot h^{-1}$). The residual carbon content in $BaTiO_3$ powder was determined using Flash EA with the method consisting in the separation of the gases by chromatography after demineralisation; a catharometer was used as detector. The elimination of carbon by thermal treatment was evidenced by mass spectrometry analysis of evolved gases coupled with TGA. Electron Paramagnetic Resonance (EPR) was performed to detect the presence of Ti^{3+} in samples, using a Bruker ESP 300 spectrometer operating at X-band frequency and 100 kHz field modulation; the samples were introduced in sealed Suprasil quartz tubes.

The $BaTiO_3$ powders prepared were uniaxially pressed at 250 MPa. The pellets (6 mm in diameter and 1.5 mm in thickness) were sintered in air at 1250 °C for 10 or 20 h (heating rate 80 °C/h). Green and fired densities were measured by the Archimede method, using water and assuming a value of 6.02 g/cm^3 for the theoretical specific mass of $BaTiO_3$. Microstructural studies of ceramics were performed using electron microscopy (Jeol JSM 6400 for SEM equipped with an energy dispersion X-ray detector). Low field electrical measurements were performed using a Hewlett Packard HP 4284A precision LCR meter. The domains explored were 20 Hz to 1 MHz for the frequency range, ambient to 160 °C for the temperature range. The voltage shape is purely sinusoidal. The applied voltage magnitude is 1 VAC.

3. Results and discussion

3.1. Powders characterization

Whatever the titanium source ($TiCl_3$ or TiO_2) and the reaction temperature (150 or 250 °C) chemical analysis data show that, on the first hand, potassium and chloride are present as traces and, on the other hand, the molar ratio Ba/Ti is very close to one. As an example, the following data, in mol%, were obtained for the BT sample prepared from $TiCl_3$ at 150 °C: Ba 50.0, Ti 49.8, K 0.06, Cl < 0.01. In agreement with Dutta [40], Cl^- ions are probably not incorporated in the BT lattice but only physisorbed.

The XRD patterns of BT samples prepared from $TiCl_3$ (Fig. 1) and TiO_2 (Fig. 2) are very similar. At first sight, it could be thought that the patterns fit well with the peak position of standard BT cubic phase (JCPDS file n° 79-2263) since the splitting of cubic peak at 2θ = 45.235° into tetragonal peaks 002 at 2θ = 44.853° and 200 at 2θ = 44° (JCPDS file n° 05-0626) is not observed. However, from a more careful examination of the patterns, two phenomena are evidenced (Table 1):

– The broadening of the peaks of a same diagram does not increase regularly with Bragg angle θ, i.e. does not obey to the Scherrer formula (1).

– For the same sample, the raise of the preparation temperature, from 150 to 250 °C, increases significantly the width of XRD peaks having different Miller indexes.

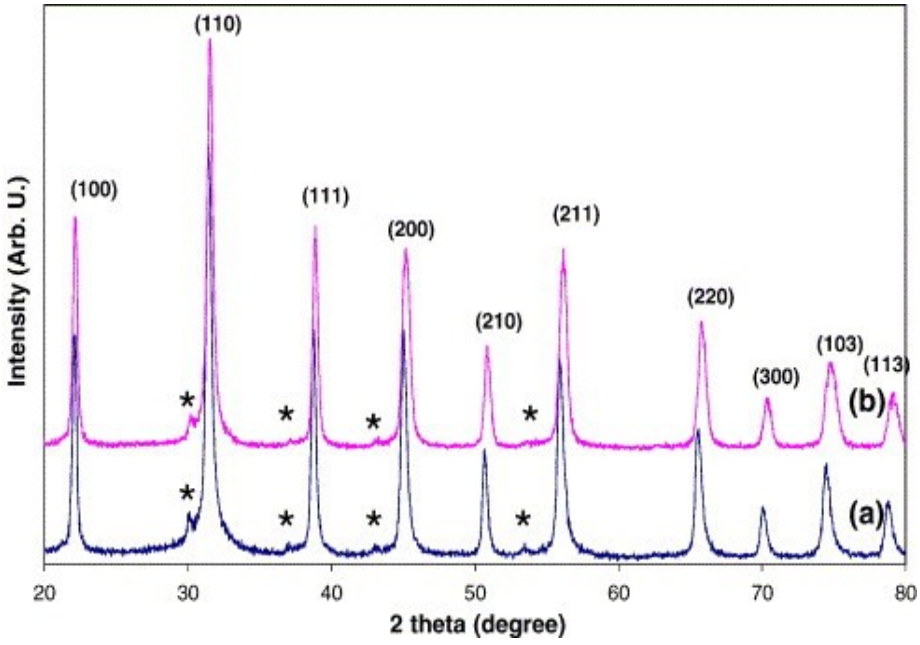

Fig. 1. X-ray diffraction patterns of $BaTiO_3$ powders prepared from $TiCl_3$ at 150 °C (a) and 250 °C (b). The given indexation corresponds to that of cubic lattice. *The small peaks are fluorescence signals coming from pollution of the copper anti-cathode by tungsten of the filament.

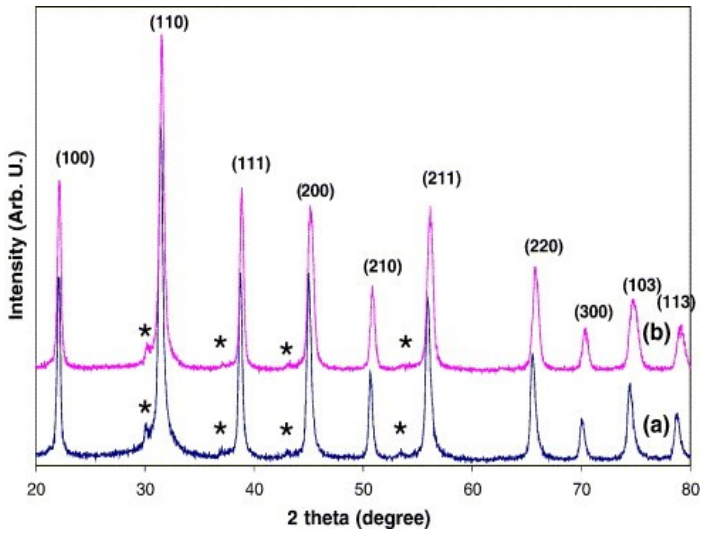

Fig. 2. X-ray diffraction patterns of $BaTiO_3$ powders prepared from TiO_2 at 150 °C (a) and 250 °C (b). The given indexation corresponds to that of cubic lattice. *The small peaks are fluorescence signals coming from pollution of the copper anti-cathode by tungsten of the filament.

Table 1.

Full-width at half-maximum of XRD peaks of BT samples

h,k,l	**FWHM (2θ°)**			
	$TiCl_3$-150 °C	**$TiCl_3$-250 °C**	**TiO_2-150 °C**	**TiO_2-250 °C**
100	0.36520	0.37460	0.31410	0.36960
110	0.48060	0.48300	0.45160	0.47840
111	0.40980	0.42100	0.37840	0.41860
200	0.48790	0.62750	0.46300	0.71520
210	0.42960	0.53170	0.37840	0.58190
211	0.53780	0.62690	0.54870	0.66170
220	0.55770	0.63240	0.54940	0.69570
300	0.56520	0.62630	0.46430	0.72160
103	0.56680	0.96110	0.57690	1.05990
113	0.61910	0.83900	0.55930	0.95820

The first observation suggests that the lattices of the studied structures, initially cubic, have undergone a low tetragonal deformation. The second one is consistent with an increase of the tetragonal deformation. Indeed the raise of the temperature should increase the crystallinity of the samples and, in absence of tetragonal deformation, a decrease of the XRD peaks width should be observed. With the recorded patterns, it is not possible to quantitatively discriminate the broadening of peaks due to the size of crystallites from the effect of the tetragonal deformation. Then, it is not possible to give an accurate value of the ratio *c*/*a* for the distorted phases.

Raman spectroscopy is a highly sensitive spectroscopic technique to probe the local structure of

atoms in materials. Based on crystallography, only infrared active bands without first-order Raman activity are predicted for cubic BT whereas eight Raman-active modes, seven of which being also IR active, are expected for tetragonal BT [32] and [43]. According to Lu [43], BT exhibits two large bands, at 520 and 716 cm^{-1} for tetragonal with nearly the same intensities. According to Busca [32], BT exhibits a band at 516 cm^{-1} for cubic and 523 cm^{-1} for tetragonal with nearly the same intensities, the stretching being a little larger for cubic; BT exhibits also a large band at 707 cm^{-1} for cubic with a significant intensity and 713 cm^{-1} for tetragonal with a strongly lower intensity. A shoulder is clearly identified at 800 cm^{-1} in the spectrum of only cubic BT. The spectra of the samples prepared from TiCl3 (Fig. 3) and from TiO_2 (Fig. 4) are very similar to the one published by Busca for cubic BT. In particular, the shoulder at 800 cm^{-1} is unambiguously discernable and the intensity of the band at 719 cm^{-1} is similar. Nevertheless, the distinction between the two polymorphs cannot be obtained only from these bands. The bands at 272 and 183 cm^{-1} bring the strongest proof of the presence of cubic BT. As for tetragonal BT, its presence is clearly shown by the narrow band at 305 cm^{-1}. The Raman spectra corroborates the XRD data, proving the existence of both cubic and tetragonal phases and indicating unambiguously that the proportion of tetragonal phase is increased by the increase of the temperature from 150 to 250 °C whatever the titanium source.

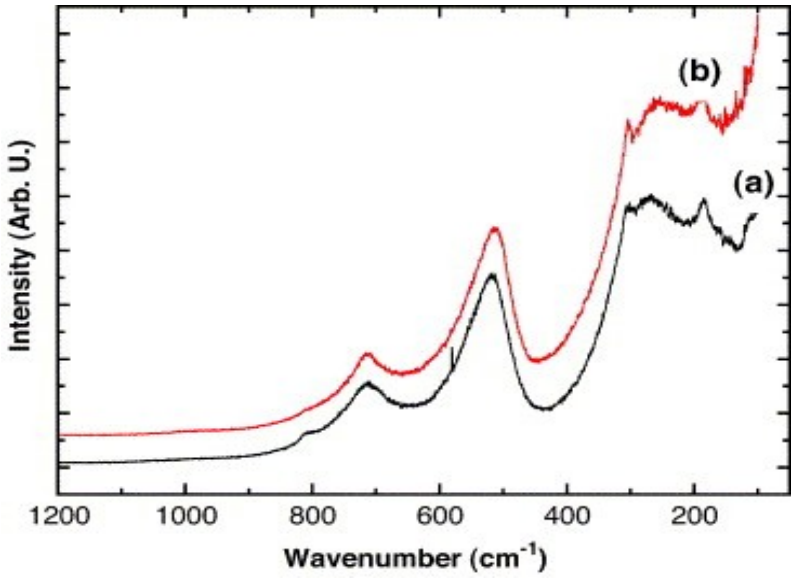

Fig. 3. Raman spectra of $BaTiO_3$ powder synthesized from $TiCl_3$ at 150 °C (a) and 250 °C (b).

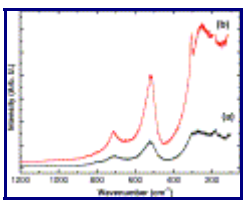

Display Full Size version of this image (23K)

Fig. 4. Raman spectra of $BaTiO_3$ powder synthesized using TiO_2 precursor at 150 °C (a) and 250 °C (b).

The nature of the titanium source and the reaction temperature have no influence on the mean size of crystallites d_x which is always close to 20 nm (Table 2). This size has been calculated according to the Scherrer's Eq. (1) from the full-width at half maximum (FWMH) of XRD peak 111 which is not splitted by the cubic to tetragonal phase transition. The geometric

surfaces (S_x) calculated from the d_x diameters are larger than the specific surface areas (S_w) measured by BET. These data agree with the formation of non-porous polycrystalline elementary grains.

Table 2.

Morphological characteristics of BT samples: mean size of crystallite d_x, geometric surface S_x and specific surface area S_w

Sample	FWMH (111) (2θ°)	2θ (°)	d_x (nm)	S_x (m^2/g)	S_w (m^2/g)
$TiCl_3$-150 °C	0.40980	38.748	21.4	49.5	16.6
$TiCl_3$-250 °C	0.42100	38.871	21.0	72.7	13.5
TiO_2-150 °C	0.37840	38.778	23.2	49.1	20.6
TiO_2-250 °C	0.41860	38.912	21.0	83.0	13.0

The FEG-SEM micrographs of BT samples, elaborated from TiCl3 (Fig. 5) and TiO_2 (Fig. 6), show spherical highly crystallized elementary grains with sizes in the range 40–70 nm for samples prepared from $TiCl_3$ at 150 °C and from TiO_2 at 150 or 250 °C and sizes in the range 80–120 nm for the sample prepared from $TiCl_3$ at 250 °C. All these sizes higher than the sizes of crystallites corroborate the formation of polycrystalline elementary grains which are more or less agglomerated. The powders prepared at 150 °C seem to be more agglomerated than the one prepared at 250 °C, particularly when $TiCl_3$ is the titanium source. One of the reasons for the formation of agglomerates could be the presence of excess of $BaCl_2$ in the reaction medium. Namely, $BaCO_3$ detected in the synthesized powders is formed during the process. The starting $BaCl_2$ solution used dos not contain $BaCO_3$ impurities. So, during the hydrothermal synthesis, retained $BaCl_2$ can absorb CO_2 and form $BaCO_3$ which might contribute to the formation of agglomerates. Dutta [46] reported that the increase of the synthesis temperature leads to an increase of the particle size which may explain agglomeration stronger at 150 °C than at 250 °C.

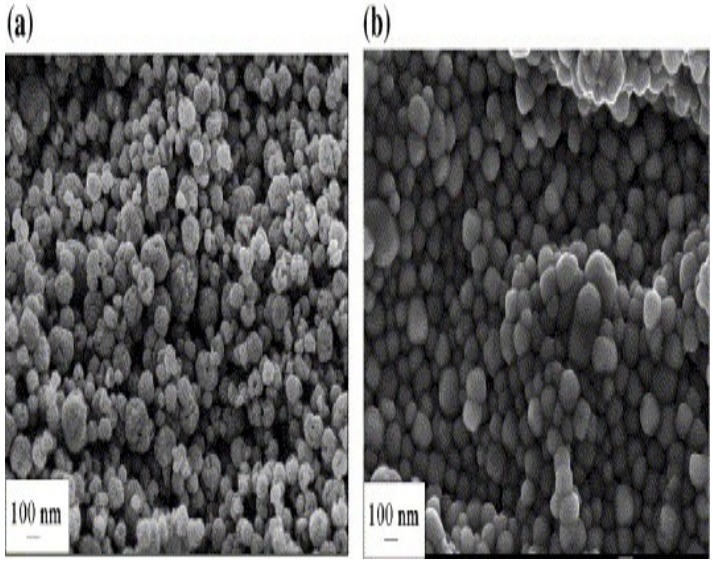

Fig. 5. FEG-SEM pictures of $BaTiO_3$ powders prepared from $TiCl_3$ at 150 °C (a) and 250 °C (b).

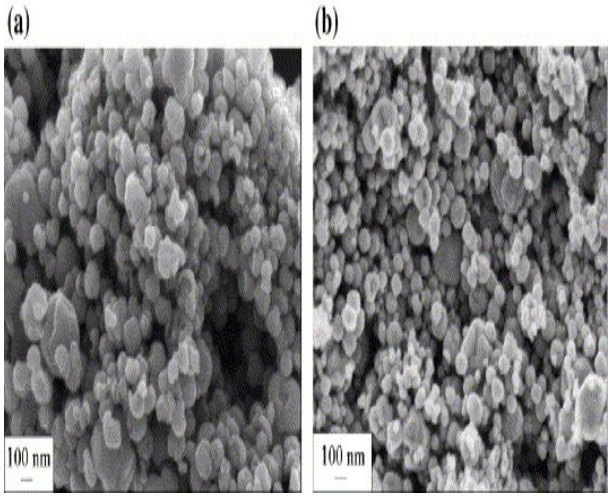

Fig. 6. FEG-SEM pictures of $BaTiO_3$ powders prepared from TiO_2 at 150 °C (a) and 250 °C (b).

TGA measurements, carried out for BT powders prepared from $TiCl_3$ (Fig. 7) and TiO_2 (Fig. 8) reveal several mass losses. A first loss, occurring in two steps below 400 °C is attributed to the release of adsorbed water, physisorbed water in the range 50–200 °C, chemisorbed water or hydroxyl groups in the range 200–400 °C. A second loss, occurring in a wide range of temperatures (400–1350 °C), results mainly from the release of CO_2 coming from the decomposition of CO_3^{2-} groups. Indeed, the release of CO_2 has been qualitatively evidenced over the whole considered temperature range by mass spectrometry analysis of the evolved gases. However, CO_2 is mostly released at temperatures over 800 °C. Similar phenomena have been observed before [47], [48] and [49]. The higher mass loss for the powders prepared at 150 °C can be understood considering that the smaller the particle size, the higher the retention of $BaCl_2$ and the concentration in OH^- defects.

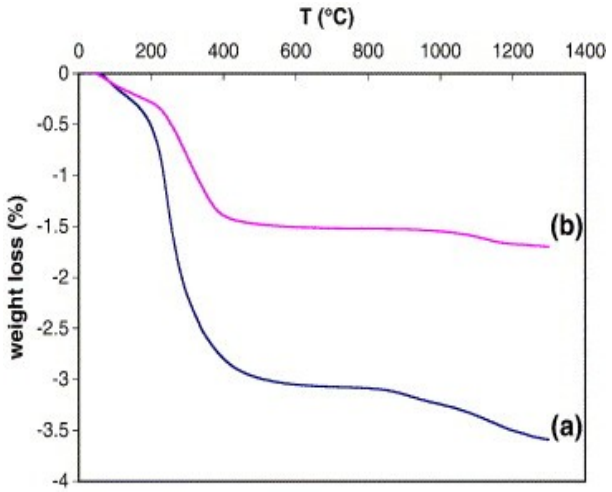

Fig. 7. Thermogravimetric analysis of $BaTiO_3$ powders synthesized from $TiCl_3$ at 150 °C (a) and 250 °C (b).

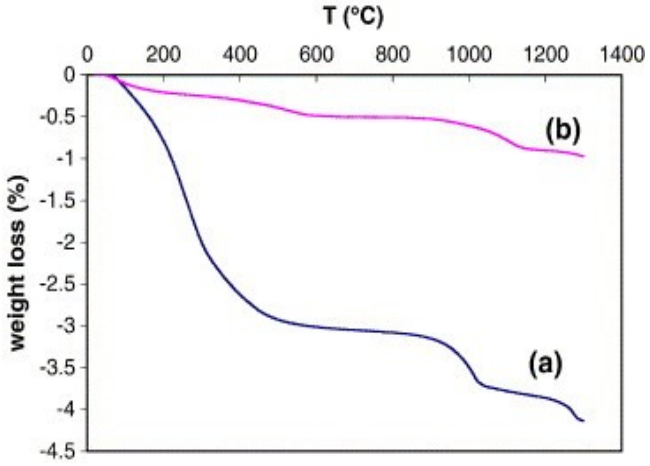

Fig. 8. Thermogravimetric analysis of $BaTiO_3$ powders synthesized from TiO_2 at 150 °C (a) and 250 °C (b).

The powders synthesized from TiO_2 are white whereas those prepared from $TiCl_3$ are yellowish. An electron paramagnetic resonance study has been undertaken in order to determine the Ti^{3+}/Ti^{4+} content. The highest common oxidation state of Ti (Ti^{4+}) is EPR silent. Only trivalent titanium with a $3d^1$ electronic configuration ($S = 1/2$) is EPR active. As expected, no EPR signal was observed for the samples synthesized from TiO_2. The EPR spectrum of a sample prepared with $TiCl_3$ as precursor (Fig. 9) shows signals, near 3500 G, typical of isolated Ti^{3+} ions. It is known that Ti^{3+} is unstable in the presence of atmospheric oxygen and oxidizes into Ti^{4+}. The small amount of Ti^{3+} detected in the powders prepared from $TiCl_3$ is significant of a non-total oxidation of Ti^{3+} to Ti^{4+}during the synthesis.

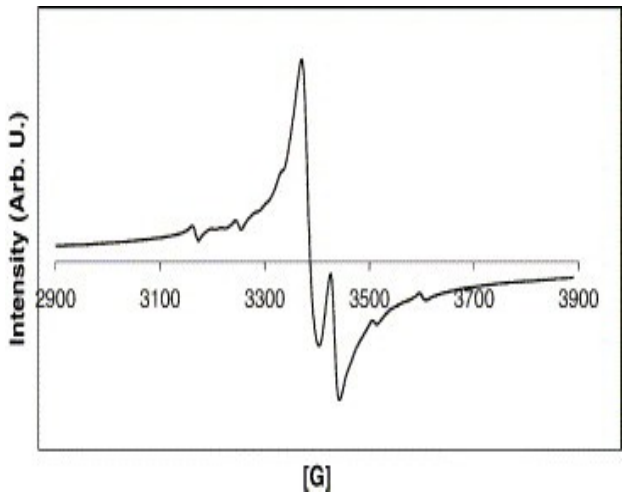

Fig. 9. EPR spectra of Ti^{3+} in $BaTiO_3$ synthesized using $TiCl_3$ as precursor.

3.2. Electrical properties of ceramics

The density values of sintered ceramics are reported in Table 3. An extension of the dwell time of sintering from 10 h to 20 h increases the densification, that reaches 99.8% in the best case. X-ray diffraction analysis only evidences tetragonal $BaTiO_3$, which is the common phase observed in such cases [50]. The tetragonal $BaTiO_3$ phase appears as the grain grows, typically above a critical size. The microstructure of $BaTiO_3$ ceramics sintered at 1250 °C for 10 h and 20 h is shown in Fig. 10 and Fig. 11. Abnormal grain growth is noticed for the sample prepared with $TiCl_3$ (synthesis temperature 150 °C or 250 °C). The microstructure of these ceramics is bimodal, constituted of large (up to 60 μm) angular grains growing in a fine-grained (1 μm) matrix. Samples of powders prepared using TiO_2 as precursor show less large grains in the fine grained matrix. The increase of the dwell time modifies the grain size and the grain size distribution, especially for powders prepared from TiO_2 (Table 2 and Fig. 11). Since the temperature of preparation does not seem to have a great influence on the powder characteristics, only the powders obtained at 250 °C (starting from $TiCl_3$ and TiO_2) have been used to prepare ceramics for the electrical properties characterization.

Table 3.

Density of the ceramics after sintering at 1250 °C during 10 and 20 h

Ti precursor	**Synthesis *T* (°C)**	**Dwell time (h)**	**% d_{th}**
$TiCl_3$	150 °C	10	98.8
		20	97.3
	250 °C	10	94.5
		20	95.6
TiO_2	150 °C	10	94.2
		20	99.8
	250 °C	10	92.2
		20	94.3

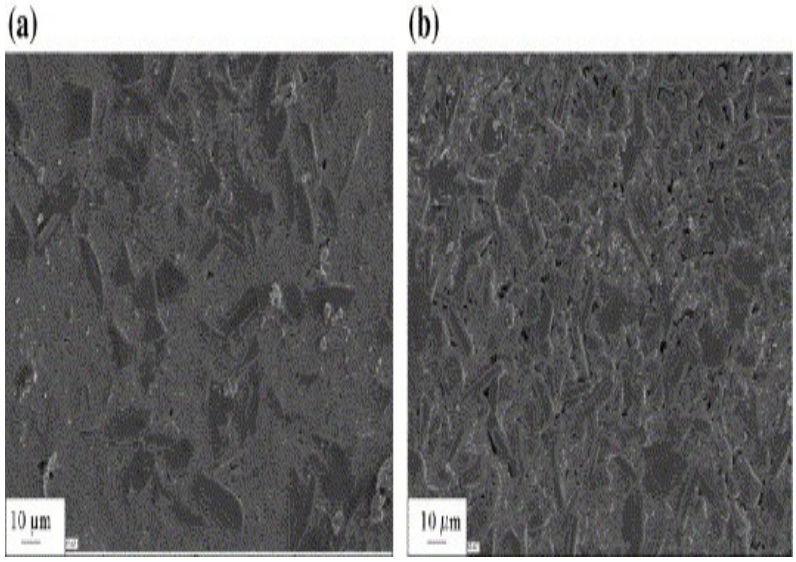

Fig. 10. SEM micrographs of $BaTiO_3$ ceramics (synthesized ex $TiCl_3$ prepared at 250 °C) sintered at 1250 °C for 10 h (a) and 20 h (b).

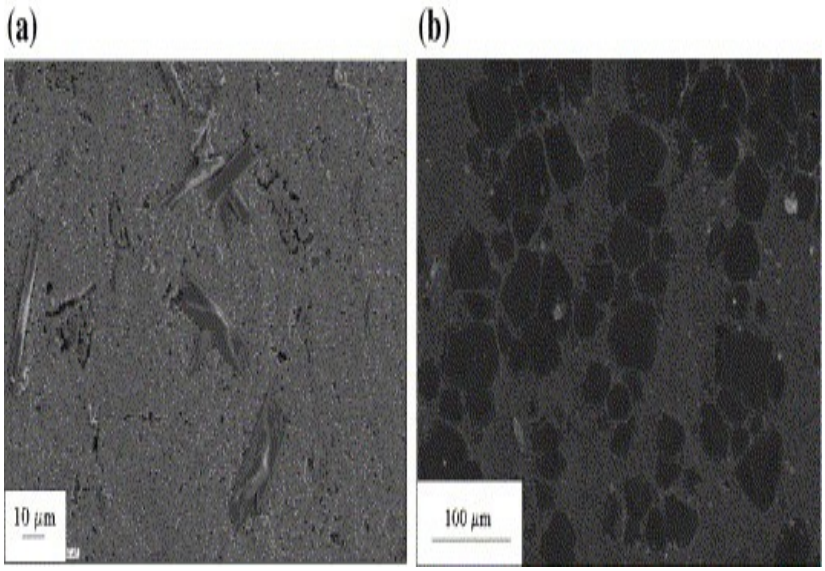

Fig. 11. SEM micrographs of $BaTiO_3$ ceramics (synthesized ex TiO_2 prepared at 250 °C) sintered at 1250 °C for 10 h (a) and 20 h (b).

The changes in the permittivity values (at 1 kHz) versus the temperature are given in Fig. 12. The first important result is that the Curie temperature (T_c) depends on the nature of the starting powders. T_c is in between 105 and 110 °C for $TiCl_3$ based ceramics whereas it is near 130 °C for TiO_2 powders based ceramics. At this temperature, the permittivity value reaches a maximum of 7000 for the former and 11,000 for the later. Whatever the ceramics, the permittivity depends on the dwell time. The value at room temperature (RT) is roughly the same whatever the dwell time for TiO_2 based ceramics, whereas at T_c a larger permittivity value is obtained for the shortest dwell time. For $TiCl_3$ starting powders based ceramics, a shift in the permittivity changes versus temperature is observed: the permittivity decreases on the whole temperature range when the dwell time increases.

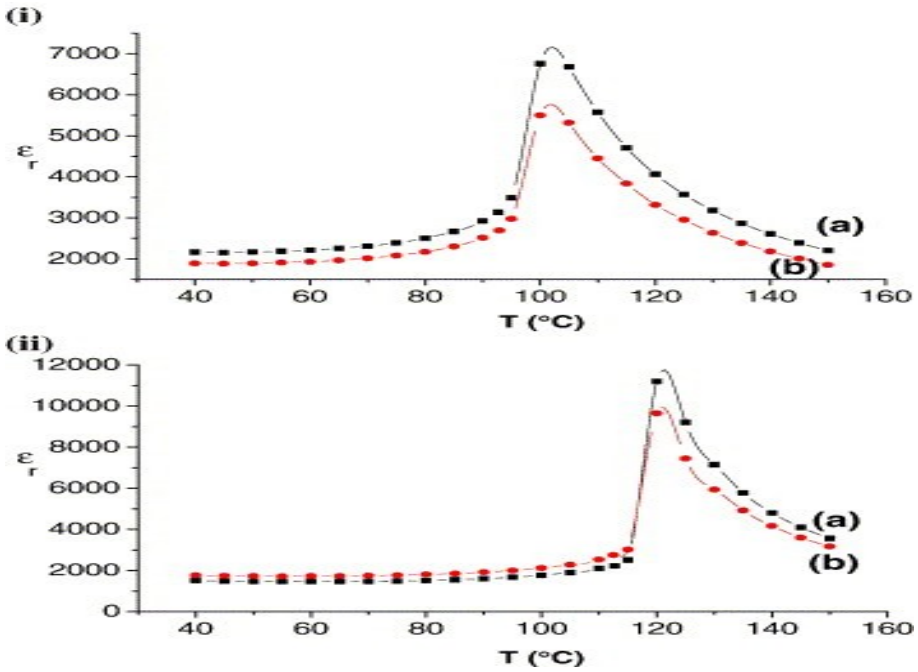

Fig. 12. Permittivity as a function of temperature (f = 1 kHz) of $BaTiO_3$ ceramics sintered at 1250 °C and prepared from powders synthesized at 250 °C for 10 h (a) and 20 h (b) using $TiCl_3$ (i) and TiO_2 (ii) as precursors.

These results are mainly related to the grain sizes and to the grain size distribution. Many studies have already been published on the size effect in ferroelectric ceramics. Kinoshita [51] and Wang et al. [52] have claimed that the finer the grain size, the higher the dielectric constant at room temperature. A value of 1 μm may be considered as an approximation of the 0.9 μm proposed by Wang, of the 0.8 μm proposed by Niepce et al. [8], of the 1 μm suggested by Duran [53] or of the 1.4 μm proposed by Hirata [54]. This behaviour is attributed to both an increase in domain wall density and to an increase in the residual internal stresses. The formation of 90° domains below T_c is the mean of minimizing this internal stress energy. Nevertheless, if grains with too small sizes are present (the width of the 90° domains being fixed near 1 μm) no 90° domain may exist and the permittivity value is decreased. In summary, the dielectric constant increases as the grain size is reduced from 10 μm to 1 μm (the maximum being obtained for 1 μm).

For the bimodal ceramics under study, the value of the dielectric constant at room temperature depends both on the amount of small sized grains and of the size distribution. Hence, for $TiCl_3$ based ceramics, the permittivity value is the largest for the smallest dwell time (10 h) for which comparable amounts of small grains with size near 400 nm and large grains with size in the range 10–20 μm coexist. The extension of the dwell time leads to an increase of the amount of 10–20 μm grains up to approximately 75% of the surface, and a diminution of ε is observed. In the case of TiO_2 based ceramics, two different situations are encountered: the presence of big grains (size 50 μm) in a finely divided matrix containing either very small grains (near 500 nm, case of TiO_2 with a dwell time of 10 h), or small grains of 1 μm mean size value (case of TiO_2 with a dwell time of 20 h). Since the ratio in the permittivity value for the grains of 500 nm and for those of 1 μm is roughly 2 [55], it is not surprising that the highest permittivity corresponds to the later.

At T_c, the contrary is observed since the maximum permittivity is obtained in the decreasing order for TiO_2, dwell time 10 h, TiO_2 dwell time 20 h, $TiCl_3$, dwell time 10 h, $TiCl_3$ dwell time 20 h.

Whatever the material under study, and even if it is not directly the same parameters which drive the properties, an increase in the amount of the big grains leads to a decrease in the permittivity value.

Lastly, as already reported by Miot [56] and Kinoshita [51], who showed that T_c increased with the grain size, the lowest T_c is obtained for the ceramics presenting the smallest grain sizes.

In conclusion, the existence of domains in ferroelectric materials which is behind the size effect seems to drive most of the electrical properties.

4. Conclusion

In summary, all the different results presented may be related to, and are explained by, the grain size and its distribution in the ceramic bulk. For small grain size with narrow grain size distribution, the permittivity at room temperature is large and the Curie temperature is 135 °C. For large grain sizes in very small grains matrix, the permittivity at room temperature is slightly larger and the phase transition is close to 110 °C.

Despite the obtention of an imperfect perovskite structure due to the presence of small amounts of Ti^{3+} in the ceramics prepared using either $TiCl_3$ or TiO_2 as titanium source, the described synthesis procedure exhibits the advantage to lead to high dielectric constants ceramics.

Acknowledgments

The authors thank Ch. Calmet for realizing the FEG-SEM pictures and A. Mari for EPR measurements.

References

P.P. Phule and S.H. Risbud, *J. Mater. Sci.* 25 (1990), p. 1169.

G. Arlt, D. Hennings and G. De With, *J. Appl. Phys.* 58 (1985), p. 1619.

S. Wada, T. Suzuki and T. Noma, *J. Ceram. Soc. Jpn.* 104 (1996), p. 383.

J.C. Niepce, *Nanomatériaux, Observatoire Français des Techniques Avancées. TEC Edition* (2001), p. 149 Paris.

D. McCuley, R.E. Newnham and C.A. Randall, *J. Am. Ceram. Soc.* 81 (1998), p. 979.

A.J. Bell, A.J. Moulson and L.E. Cross, *Ferroelectrics* 54 (1984), p. 147.

M.R. Shrinivasan, M.S. Multani Ayyub, P. Ayyub and R. Vuayaraghavan, *Ferroelectrics* 51 (1983), p. 137.

G. Caboche, F. Chaput, J.P. Boilot and J.C. Niepce, *Silic. Ind.* 5–6 (1993), p. 103.

C. Valot-Odot, Phd Thesis, Dijon, 1996.

H.I. Hsiang and F.S. Yen, *J. Am. Ceram. Soc.* 79 (1996), p. 1053.

N. Bernaben, A. Leriche, B. Thierry, J.C. Nièpce and R. Waser, *Fourth Euro Ceramics* vol. 5 (1995), p. 203.

A. Beauger, J.C. Moutin and J.C. Niepce, *J. Mater. Sci.* 18 (1983), p. 3041.

D.F.K. Hennings, B.S. Schreinemacher and H. Schreinemacher, *J. Am. Ceram. Soc.* 84 (2001) (12), p. 2777.

M.H. Frey and D.A. Payne, *Phys. Rev., B* 54 (1996), p. 3158.

S. Schlay and H.F. Eicke, *Solid State Commun.* 91 (1994), p. 883.

R.N. Viswanath and S. Ramasamy, *Nanostruct. Mater.* 8 (1997), p. 155.

H. Shimoaka and M. Kwabara, *J. Am. Ceram. Soc.* 79 (1996), p. 2983.

G. Plaff, *J. Mater. Chem.* 2 (1992), p. 591.

T. Takeuchi, M. Tabuchi, K. Ado, K. Honjo, O. Nakamura and H. Kagasawa, *J. Mater. Sci.* 32 (1997), p. 4053.

S. Wada, T. Hoshina, H. Yasuno, S.M. Nam, H. Kakemoto and T. Tsurumi, Electroceramics in Japan, *Key Eng. Mater.* 19 (2003), p. 248.

Ch. Beck, W. Hartl and R. Hempelman, *J. Mater. Res.* 13 (1998), p. 3174.

J. Wang, J. Fang, S.C. Ng, L.M. Gan, C.H. Chew, X. Wang and Z. Shein, *J. Am. Ceram. Soc.* 82 (1999), p. 873.

W.S. Cho, *J. Phys. Chem. Solids* 59 (1998), p. 659.

D. Hennings, G. Rosenstein and H. Schreinemacher, *J. Eur. Ceram. Soc.* 8 (1991), p. 107.

M. Wu, R. Xu, S.H. Feng, L. Li, D. Chen and Y.J. Luo, *J. Mater. Sci.* 31 (1996), p. 6201.

C.T. Xia, E.W. Shi, W.E. Zhong and J.K. Guo, *J. Eur. Ceram. Soc.* 15 (1995), p. 1171.

J.O. Eckert Jr., C.C. Hung-Houston, B.L. Gersten, M.M. Lencka and R.E. Riman, *J. Am. Ceram. Soc.* 79 (1996), p. 2929.

E.B. Slamovich and I.A. Aksay, *J. Am. Ceram. Soc.* 79 (1996), p. 239.

A.N. Christensen, *Acta Chem. Scand.* 24 (1970), p. 2447.

L. Zhao, A.T. Chien, F.F. Lapse and J.S. Speck, *J. Mater. Res.* 11 (1996), p. 1325.

R. Viekanandan and T.R.N. Kutty, *Powder Technol.* 57 (1989), p. 181.

G. Busca, V. Buscaglia, M. Leoni and P. Nanni, *Chem. Mater.* 6 (1994), p. 955.

T. Noma, S. Wada, M. Yano and T. Suzuki, *J. Appl. Phys.* 80 (1996), p. 5223.

R. Asiaie, W. Zhu, S.A. Akbar and P.K. Dutta, *Chem. Mater.* 8 (1996), p. 226.

I.J. Clark, T. Takeuchi, N. Othori and D.C. Sinclair, *J. Mater. Chem.* 9 (1999), p. 83.

D. Hennings and S. Schreinemarcher, *J. Eur. Ceram. Soc.* 9 (1992), p. 41.

J. Menashi, R.C. Reid, L. Wagner, Cabot Corporation, US patent 4829033, May 9, (1989).

E.W. Shi, C.T. Xia, W.E. Zhong, B.G. Wang and C.D. Feng, *J. Am. Ceram. Soc.* 80 (1997), p. 1567.

B.D. Begg, E.R. Vance and J. Nowotny, *J. Am. Ceram. Soc.* 77 (1994), p. 3186.

P.K. Dutta and J.R. Gregg, *Chem. Mater.* 4 (1992), p. 883.

R. Vivekanandan, S. Phillip and T.R.N. Kutty, *Mater. Res. Bull.* 99 (1986), p. 22.

C.T. Xia, E.W. Shi, W.Z. Zhong and J.K. Guo, *J. Cryst. Growth* 166 (1996), p. 961.

S.W. Lu, B.I. Lee, Z.L. Wang and W.D. Samuels, *J. Cryst. Growth* 219 (2000), p. 269.

B.D. Cullity, Elements of X-ray Diffraction, Addison Wesley, Reading, MA (1978).

L.L. Hench and J.K. West, *Principles of Electronics Ceramics*, Wiley, New York (1990), p. 246.

P.K. Dutta, R. Asiaie, S.A. Akbar and W. Zhu, *Chem. Mater.* 6 (1994), p. 1542.

B.L. Newalkar, S. Komarneni and H. Katsuki, *Mater. Res. Bull.* 36 (2001), p. 2347.

C. Proust, C. Miot and E. Husson, *J. Eur. Ceram. Soc.* 15 (1995), p. 631.

S. Urek and M. Drofenik, *J. Eur. Ceram. Soc.* 18 (1998), p. 279.

M.B. Park, S.J. Hwang and N.H. Cho, *Mater. Sci. Eng., B, Solid-State Mater. Adv. Technol.* 99 (2003), p. 155.

K. Kinoshita and A. Yamaji, *J. Appl. Phys.* 47 (1976) (1), p. 371.

X.H. Wang, R.Z. Chen, Z.L. Gui and L.T. Li, *Mater. Sci. Eng., B, Solid-State Mater. Adv. Technol.* 99 (2003), p. 199.

P. Duran, D. Gutierez, J. Tartaj and C. Moure, *Ceram. Int.* 28 (2002), p. 283.

H. Hirata, A. Nitta, S. Sameshina and K. Kamino, *Mater. Sci. Lett.* 29 (1996), p. 229.

H.S. Nalwa, *Handbook of Low and High Dielectric Constant Materials and Their Applications* vol. 2 (1999), p. 61.

C. Miot, C. Proust and E. Husson, *J. Eur. Ceram. Soc.* 15 (1995), p. 1163.

Corresponding author. Tel.: +33 561 556 283; fax: +33 561 556 163.

Original text : Elsevier.com